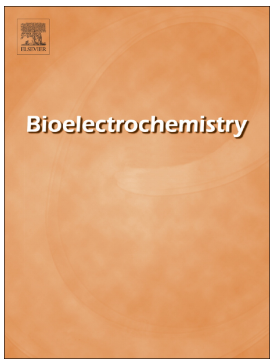

Fabrication of a κ-carrageenan-based electroactive cytochrome c multilayer thin film by an electrostatic layer-by-layer assembly

Zülfikar Temoçin

PII: S1567-5394(18)30378-5
DOI: https://doi.org/10.1016/j.bioelechem.2019.04.021
Reference: BIOJEC 7291

To appear in: *Bioelectrochemistry*

Received date: 27 August 2018
Revised date: 27 April 2019
Accepted date: 27 April 2019

Please cite this article as: Z. Temoçin, Fabrication of a κ-carrageenan-based electroactive cytochrome c multilayer thin film by an electrostatic layer-by-layer assembly, Bioelectrochemistry, https://doi.org/10.1016/j.bioelechem.2019.04.021

Fabrication of a κ-carrageenan-based electroactive cytochrome *c* multilayer thin film by an electrostatic layer-by-layer assembly

Zülfikar Temoçin

Department of Chemistry, Faculty of Arts and Sciences, Kırıkkale University, Yahşihan,71450 Kırıkkale, Turkey

Email: ztemocin@kku.edu.tr

Abstract

The aim of this study was to demonstrate the usability of κ-carrageenan in the accumulation of a layer by layer protein film on a gold electrode. It is known that in terms of bioelectronics there are significant advantages to functional biofilms which are formed as a result of the interaction between different layer biomolecules. In this study, κ-carrageenan (κ-CG) was employed as the polyanion for the construction of the electroactive multilayer protein thin films. The protein layers were built up by successive adsorption of κ-CG and cytochrome *c* (cyt *c*) based on the opposite charge on a modified gold electrode with a cyt *c* monolayer. Electron transport between the cyt *c* layers was established without the hindrance of κ-CG. The highest electron transfer capability was achieved when the pH value of the solutions was 5, and the κ-CG concentration was a 0.25 mg mL^{-1}. Whilst the amount of cyt *c* on the electrode surface was 10.87 pmol cm^{-2} in the monolayer structure, the amount was calculated to be 158.01 pmol cm^{-2} with the formation of 8-bilayer [κ-CG/cyt *c*] structures over the cyt *c* monolayer. The multilayer protein film was also characterized using electrochemical impedance spectroscopy, ellipsometry, and UV-visible absorption spectroscopy. This novel biofilm allows a high amount of electron transfer and can be used as an immobilization platform for biosensor applications.

Keywords: carrageenan; cytochrome *c;* multilayer film; electron transfer; electrostatic interaction

1. Introduction

Coupling of the molecular recognition properties of biomolecules with the signal transduction capabilities of electronics could be possible if proteins were immobilized on electrode surfaces in suitable microenvironments where the labile biological components are protected [1-5]. Either a shuttle molecule or a direct electron transfer method can be employed to establish electronic communication between the electrodes and proteins [6-8]. Several strategies for direct electron transfer have been attempted such as the use of genetically engineered enzymes [9,10] and specifically designed electrode surfaces [8,11,12] for the fabrication of efficient electrochemical biosensors.

If direct electron transfer is established between redox protein and electrode, the use of redox mediators can be avoided, thus reducing potential interference and side reactions. However, only some redox proteins show efficient direct electron transfer [13,14]. One of these proteins is cytochrome *c (*cyt *c)*, which allows heterogeneous electron transfer at a gold electrode [15,16]. Cyt *c* has been immobilized on the electrode surfaces by different techniques such as physical adsorption [17], entrapment [18], layer-by-layer assembly (LBL) [19], Langmuir–Blodgett [20], and covalent attachment [21]. For instance, LBL assembly is employed to produce supramolecular hybrid multilayer models under mild conditions as this is particularly important for preserving the activity of the biomolecules [22-24]. This method allows an increase in protein content on the electrode surface. However, the critical point is to obtain effective electron transport through the protein-polyelectrolyte assembly to the electrode [25].

The isoelectric point of cyt *c* is about 10, and below this pH value, cyt *c* is charged positively. This positive charge allows the protein to attach or to interact with negatively charged groups on the surfaces of the other molecules [26,27]. For example, the sulfonated polyaniline was used as a counter polyelectrolyte for multilayer assembly of cyt *c* [28]. In another study, a fully electroactive protein multilayer electrode based on DNA and cyt *c* was constructed [29]. A more complicated approach is the multilayer immobilization of cyt *c* and a redox enzyme on gold substrates. This structure does not require a shuttle molecule to allow electron transfer between the electrode and the redox enzyme. Cyt *c* is employed as an electron provider in the multilayered structure, transferring electrons from the electrode to the enzyme [30-33]. These findings are significant for two reasons: First, they indicate the compatibility of cyt *c* with redox enzymes, which allows direct electron transferring within a polyelectrolyte multilayer structure, combining cyt *c* and the redox enzyme. Second, the catalytic current necessary for the biosensor sensitivity increases due to the growing number of accumulated layers in the constructed artificial biprotein multilayer system. That is why a cyt *c* multilayer system is valuable for the development of third-generation biosensors [34,35]. Therefore, preparation of multilayered architecture of cyt *c* with different polyelectrolytes is important in terms of assessing the compatibility of polyelectrolytes with cyt *c* in multilayered architecture.

Carrageenan is the name for a family of high molecular weight sulphated polysaccharides obtained by extraction of certain species of red seaweeds. It is composed of galactose and anhydrogalactose units linked by glycosidic unions. It can be traditionally split into six basic forms: Kappa, Iota, Theta, Mu, Nu and Lambda

carrageenan [36]. Of these different types of carrageenan, kappa-carrageenan (κ-CG) is the most used one in the combinations of carrageenan with other polymers [37-40]. However, to the best of my knowledge, the κ-CG and cyt *c* have not been studied together in the experimental research so far.

In this paper, κ-CG was employed for multilayer immobilization of the electroactive cyt *c* on a gold wire electrode. The electron transfer capacity of this multilayered system was measured. To establish this system, cyt *c* monolayer was immobilized on the gold wire electrode modified with alkanethiols [41]. Then, the assembly capabilities of κ-CG were investigated on LBL immobilization of cyt *c* for such conditions as solution pH values, κ-CG concentration and incubation time.

2. Materials and Methods

2.1. Materials

Horse-heart cytochrome c, 11-mercapto-1-undecanoic acid (MUA) and 11-mercapto-1-undecanol (MU) were purchased from Sigma-Aldrich. κ-Carrageenan was provided from Fluka. Potassium hydroxide, hydrogen peroxide, and ethanol were purchased from Panreac. Sodium hydroxide, sodium dihydrogen phosphate, phosphoric acid, sulfuric acid, potassium ferricyanide, potassium ferrocyanide, and nitric acid were supplied from Merck. The gold wire electrodes (0.5 mm diameter) were provided from Alfa Aesar. The gold sheets (1 cmx1cm) were supplied from a local vendor. All solutions were prepared with deionized water by Elga Pure Lab Classic.

2.2. Solutions

The solutions of 5 mM MUA and 5 mM MU were separately prepared in ethanol and stored at +4 °C. The 5 mM phosphate buffer pH 7.0 solution was used for the preparation of cyt *c* solution (30 µM) and as the electrolyte solution for the electrochemical measurements. The 0.5 mM phosphate buffer solution was used for the preparation of the κ-CG, cyt *c* (20 µM) and as the rinsing solution [25]. The κ-CG was dissolved in the 0.5 mM sodium phosphate buffer solution at 80 °C.

2.3. Immobilization of cyt *c* monolayer

Gold electrodes were cleaned as described in the method of Katz et al [42]. They were incubated in piranha solution [H_2SO_4: H_2O_2 (3:1, v/v)] for 10 min. Then they were boiled in KOH solution (2.5 M) for 4 hours. Finally, they were incubated in concentrated nitric acid for 10 min, having been kept in concentrated H_2SO_4 for overnight. The electrodes were carefully rinsed with deionized water after each step. The cyt *c* monolayer was prepared according to a previously published procedure [41]. The cleaned gold electrodes were incubated in a mixture containing 5 mM MUA and 5mM MU (ratio 1:3) for 48 h. Having been rinsed carefully with ethanol and deionized water, they were incubated in cyt *c* solution (30 µM) for 2 h and finally rinsed carefully with the 5 mM phosphate buffer solution.

2.4. Multilayer immobilization of cyt *c*

As described above, the freshly prepared monolayer electrodes were successively incubated in the κ-CG solution and the cyt *c* solution (20 µM in 0.5 mM phosphate buffer) and carefully rinsed three times in 0.5 mM phosphate buffer after each step [43].

Multilayer κ-CG/cyt *c* thin films on gold sheets were prepared for ellipsometric measurement with the same manner as described above for the gold wire electrodes.

For UV-vis absorption measurement, the κ-CG film (about 0.5 mm thickness) was prepared by drying the κ-CG solution (2%) in a petri dish for 48 h at 40 °C. Then the κ-CG film was cut into test sections in appropriate sizes (about 1cmx2cm). Two of the test sections were incubated in the cyt c solution (20 µM in 0.5 mM phosphate buffer) for the preparation of cyt *c* monolayered κ-CG film. To prepare the 8-bilayer κ-CG/cyt *c* film, the cyt *c* monolayered κ-CG film was consecutively incubated in the κ-CG and cyt *c* solutions and carefully rinsed three times in the 0.5 mM phosphate buffer solution after each step. The films were dried at room temperature before UV-vis absorption measurement.

2.5. Electrochemical measurements

Cyclic voltammetry (CV) and electrochemical impedance spectroscopy (EIS) experiments were performed with the aid of a CHI 660B (CH Instrument, USA) electrochemical workstation. Electrochemical measurements were carried out in 1 mL of sodium phosphate buffer solution (5 mM, pH 7.0). A commercial Ag/AgCl (3 mol L^{-1} KCl) electrode (CHI) was used as the reference and a Pt wire was used as the counter electrode [25]. The working electrode was a modified gold wire one. The CV measurements were performed at a scan rate of 0.1 V s^{-1} for multiple cycles (between +0.25 V and -0.25 V). The experiments were conducted for three replicates to confirm the results. The amount of immobilized cyt *c* (Γ) on the gold surface was calculated by the following equation:

$$\Gamma = {}^{Q}/_{nFA} \quad (1)$$

where Q is the charge (average of the anodic and cathodic charge values), n is the number of electrons, F is Faraday constant and A is the area of the electrode surface. Here, the charge (Q) is determined by integrating the peak area of cyclic voltammogram.

The frequency range used for the EIS measurements, which were performed in the phosphate buffer solution (5 mM, pH 7.0) containing 1 mM $K_3Fe(CN)_6$ and 1 mM $K_4Fe(CN)_6$ with an amplitude of 0.025 V, was from 100 kHz to 0.05 Hz. The pure argon was used to deoxygenate the solution before measurements were performed.

2.6. Characterization of multilayer κ-CG/cyt *c* structure

The ellipsometric measurements of the multilayer κ-CG/cyt *c* film on the gold sheets were recorded by a J.A. Woollam Co., Inc. HS 190 (Nebraska, USA) spectroscopic ellipsometer (V-VASE, angle:75º). The optical constants and the thickness of multilayer thin films were fitted using the Cauchy model.

UV–visible (UV-vis) absorption spectra of the cyt *c* solution and the films were recorded with a Perkin Elmer Lambda 35 (USA) spectrophotometer.

3. Results and Discussion

The use of the LBL assembly technique based on the interaction of cyt *c* with polyelectrolytes and nanoparticles allows more cyt *c* to be immobilized on the electrode surface. The combination of this form of cyt *c* with enzymes provides new bioelectronic functionalities [44-46]. Thus, in this research, the interaction between κ-CG and cyt *c* has been investigated by composing an electroactive cyt *c* multilayer system as illustrated in Schematic 1. This interaction between κ-CG and cyt *c* was identified by the cyclic voltammetry technique, exploiting the electroactive properties of cyt *c* [47,48].

Schematic 1

In the initial step of this work, the cyt *c* monolayer was prepared on the gold electrode. Fig. 1a displays cyclic voltammogram of the immobilized cyt *c* monolayer on the gold electrode. In this voltammogram, the peak currents were observed near +0.015 V for oxidation of cyt *c* and +0.010 V for reduction of cyt *c*. The amount of electroactive cyt *c* in monolayer immobilized system was calculated to be 10.8 pmol cm^{-2}. The cyclic voltammogram of the immobilized cyt *c* monolayer with multiple cycles is replotted as time-current curves in Fig. 1b, which illustrates that the monolayer of cyt *c* was steady over multiple cycles with little change in peak currents.

Fig. 1a and b.

3.1. Effect of solution pH values on intermolecular interaction for construction of 2- bilayer [κ-CG/cyt *c*] structures

The multilayer system was formed on cyt *c* monolayered electrode by consecutive adsorption of the κ-CG as the polyanion and cyt *c* as the polycation. The solution pH is a key factor for the interaction between different molecules due to the variation of the magnitude of the electrical charge of dissolved molecules. This fact directly affects the electrostatic interaction between molecules, changing the adsorption process and the film properties [49,50]. The solutions of κ-CG (0.2 mg mL^{-1}) and cyt *c* (20 μM) with different pH values (pH 4.0, 5.0, 6.0, and 7.0) were prepared (in 0.5 mM phosphate buffer) to investigate the effect of solution pH values on the electrostatic interactions of κ-CG and cyt *c*. The cyt *c* monolayered gold electrode was incubated in κ-CG and then cyt *c* solution for 10 min. The cyclic voltammograms of pH-dependent 2-bilayer κ-CG/cyt *c* films are given in Fig 2a. The amounts of immobilized cyt *c* on the electrode surface calculated from voltammograms are shown in Fig 2b. As observed from each peak current value in the voltammograms, the highest amount of electron transfer from the oxidation and reduction of cyt *c* was obtained from the multilayer κ-CG/cyt *c* film prepared at pH 5.0. It shows that the best interaction between the κ-CG and cyt *c* occurs at pH 5.0. One other result obtained from voltammograms is that at pH 6.0, and 7.0, the formation of the bilayer κ-CG/cyt *c* structure could be observed, whilst at pH 4.0, no bilayer κ-CG/cyt *c* structure was formed despite the increase in the positive charge density of cyt *c*. In fact, it is known that decreasing the pH value of the solution causes an increase in the magnitude of the positive charge of the proteins due to the protonation of the side chain of amino acids [51]. Why a bilayer κ-CG/cyt *c* film was not formed at pH 4.0 might be due to the change in κ-CG ionic structure. At this pH value, partial protonation may take place in the κ-CG structure. Thus, there may be a reduction in the negative charge density of the sulfate group which provides electrostatic interaction with other

molecules on the κ-CG surface [52]. The next multilayer κ-CG/cyt *c* structures were formed at pH 5.0.

To provide evidence for the deposition of cyt *c* and κ-CG on the cyt *c* monolayered electrode by LBL assembly, the cyt *c* monolayered electrode was incubated in a solution (pH 5.0) containing cyt c (20 μM) and κ-CG (0.2 mg mL^{-1}). The voltammograms of this new electrode, the 2-bilayer κ-CG/cyt *c* electrode (prepared by LBL) and the cyt *c* monolayered electrode were given in Fig. 2c. When the voltammograms are compared, it is seen that the electrode incubated in a solution containing cyt *c* and κ-CG has even lower peak currents than the cyt *c* monolayered electrode. This result indicates that if the cyt *c* and κ-CG are found in the same solution, cyt c cannot be deposited on the cyt *c* monolayered electrode. In addition, the electron transfer capacity of the cyt *c* monolayered electrode was adversely affected by the incubation technique in a solution containing cyt *c* and κ-CG.

Fig. 2a, Fig. 2b and Fig. 2c

3.2. Effect of incubation time of the gold monolayered electrode on intermolecular interaction for construction of 2-bilayer κ-CG/cyt *c* film

To investigate the effect of the incubation time of the gold electrodes in solutions on the construction of multilayer electroactive protein architecture, the modified gold electrodes were incubated in the κ-CG solution first and then in the cyt *c* solution for different time periods (2.5, 5, 10 and 20 min). The cyclic voltammograms of the 2-bilayer κ-CG/cyt *c* films prepared in different incubation times were given in Fig 3a. As can be seen from the voltammograms, the peak currents of the multilayer κ-CG/cyt *c* structures showed an increase with the increase of the incubation time. The amounts of immobilized electroactive cyt *c* on the electrode surface calculated from voltammograms are shown in Fig 3b. The results show that the deposition of κ-CG and cyt *c* on each other is almost completed in 5 minutes. Although the highest peak current is obtained for 20 min incubation time, the successive voltammograms show that the stability of this multilayer film is somewhat low (Figure is not given). The subsequent multilayer films were prepared for 10 min of incubation time.

Fig.3a and Fig. 3b

3.3. Effect of κ-CG concentration on intermolecular interaction in the construction of 3-bilayer κ-CG/cyt *c* structure

The effect of κ-CG concentration on the formation of a multilayer κ-CG/cyt *c* architecture was investigated. The cyt *c* monolayered gold electrodes were incubated in κ-CG solutions with different concentrations and then in the cyt *c* solutions (20 μM). The cyclic voltammograms of the 3-bilayer artificial architecture of κ-CG/cyt *c* were given in Fig 4a. As can be seen from the voltammograms, when the κ-CG concentration is increased from 0.1 mg mL^{-1} to 0.25 mg mL^{-1}, there is a considerable increase in the peak currents for the oxidation and reduction of the accumulated cyt *c* in the multilayer system. However, when the κ-CG concentrations were 0.5 mg mL^{-1} and 1 mg mL^{-1}, there was a gradual decrease in the oxidation and reduction peak currents of the cyt *c* in the multilayer system. The amounts of immobilized electroactive cyt *c* on the electrode surface calculated from voltammograms are shown in Fig 4b. The decrease in the amount of electroactive protein on electrode surface depending on the increase in κ-CG concentration (0.5 mg mL^{-1} and 1 mg mL^{-1}) can be attributed to the increase in the ionic strength [29]. These results indicate

that the optimum κ-CG concentration for the most stable interaction between κ-CG and cyt *c* is 0.25 mg mL^{-1}. The subsequent multilayer films were prepared with 0.25 mg mL^{-1} of κ-CG concentration.

Fig.4a and Fig. 4b

3.4. The Building up of the multilayer κ-CG/cyt *c* system

The multilayer film of the bilayer κ-CG/cyt *c* was prepared using the optimum conditions set out above on the interaction between κ-CG and cyt *c*. For this purpose, the cyt *c* monolayered gold electrodes were incubated in κ-CG solutions (0.25 mg mL^{-1}, pH 5.0) for 10 min and then in the cyt *c* solutions (20 μM, pH 5.0) for 10 min. As can be seen from Fig. 5a, the intensity of the oxidation and reduction peak currents of the cyt *c* increased as the numbers of κ-CG/cyt *c* layers formed on the electrode surface were increased. The cyclic voltammograms of the 8-bilayer κ-CG/cyt *c* film were replotted as time-current curves (Fig. 5a inset), which illustrates that the multilayer κ-CG/cyt *c* film was steady over multiple cycles with little change in the peak currents. The amounts of immobilized electroactive cyt *c* on the electrode surface calculated from voltammograms are shown in Fig 5b. Whilst the amount of electroactive monolayer of the cyt *c* was 10.87 pmol cm^{-2} on the gold electrode, this value reached 158.01 pmol cm^{-2} in the 8-bilayer κ-CG/cyt *c* system constructed using κ-CG. In addition, as the number of bilayer κ-CG/cyt *c* on the electrode surface increases, the anodic and cathodic peak potentials of the cyt *c* have been separated (Fig. 5c). A similar observation has been pointed out in the literature for the DNA-cyt *c* multilayer structure. It has been noted that the electron transfer kinetics is subject to a limitation of the assembled proteins [29].

Fig.5a, Fig 5b, and Fig. 5c

To provide more definitive evidence for the electron transfer kinetics of the multilayer structure, a 4-bilayer κ-CG/cyt *c* film was used for the evaluation of the shift of the peak potential with respect to the scan rate in the cyclic voltammograms. It was observed that the increase in the scan rate caused peak separation (Fig. 6) and a linear increase of the redox peak currents (Fig. 6 inset). The calculation of the rate constant (k_s) for the electron transfer between the multilayer film and the electrode was performed according to the Laviron equation, considering the scan-rate dependence of the anodic and cathodic peak potentials: in the event of $n\Delta E_p \leq 0.2$ V [53, 54]

$$k_s = {}^{mnvF}/_{RT} \qquad (2)$$

where m is a parameter related to the ΔE_p (it is obtained from ref. 53), n is the number of the electron transferred (for cyt *c* it is known as 1), R is the gas constant, T is the temperature, and v is the scan rate and F is the Faraday constant [54]. The electron transfer rate constant k_s was calculated to be 3.11 ± 0.26 s^{-1} at a scan rate of 0.1 V s^{-1}.

However, the electron transfer rate of cyt *c* monolayer had been reported to be 75 s^{-1} [43]. Clearly, the electron-exchange rate between the protein molecules in the multilayer protein system is notably slower than the electron transfer rate of the cyt *c* monolayer on the gold electrode. It can be concluded that the peak separation of multilayer κ-CG/cyt *c* structure is related to the electron transfer kinetics between protein molecules.

Fig.6

3.5. Characterization of the multilayer κ-CG/cyt *c* system

In the next set of experiments, the multilayer κ-CG/cyt *c* system was characterized by EIS. The Nyquist curves were plotted for bare gold, monolayer cyt *c* and multilayer κ-CG/cyt *c* films (2-bilayer, 4-bilayer, 6-bilayer, and 8-bilayer), as illustrated in Fig. 7. It is clear from the figure that the increase in the number of cyt c layers created differences in Nyquist curves for monolayer and multilayer protein films. The Nyquist plot of the bare gold electrode, found to be almost linear, demonstrated that the transfer of charges was unhindered. After the assembly of the cyt *c* monolayer and κ-CG/cyt *c* bilayers on the gold electrode, the Nyquist plots exhibited a semicircular shape at low frequency, which indicates that the addition of the cyt *c* monolayer and κ-CG/cyt *c* bilayer hinders the diffusion of $Fe(CN)_6^{3-/4-}$ to the gold electrode surface. With each subsequent cyt *c* assembly step, Fig. 7 shows that the semicircle diameter of the Nyquist plot increases, which indicates increasing charge transfer resistance. This expansion in the semicircle diameter of the Nyquist curves can be attributed to the poor electrical conductivity of cyt *c* [55]. Another possible cause for the increase in the charge transfer resistance could be the repulsive electrostatic interaction between the negatively charged κ-CG and $Fe(CN)_6^{3-/4-}$ [56,57]. The Randles circuit (Fig. 7 inset) was evaluated to be the best fit for the impedance data.

Fig.7

Ellipsometry is a method widely used to study the characteristics of thin films onto modified surfaces [58]. The thickness of the multilayer κ-CG/cyt *c* film for 4-bilayer and 8-bilayer films were probed using ellipsometry. The fitting was done by minimizing the mean-square error calculated by ellipsometer's own computer program, using the Cauchy model. The spectral variations of the ellipsometric angles were presented in Fig. 8. The multilayer film thicknesses from the ellipsometric data were calculated to be 15.019±1.36 nm and 26.398±1.52 nm for 4-bilayer κ-CG/cyt *c* and 8-bilayer κ-CG/cyt *c* films respectively. The increase in the film thickness due to the increase in the number of bilayers κ-CG/cyt *c* shows that the κ-CG/cyt *c* multilayer film was formed on the gold surface [59].

Fig.8

Fig. 9 shows the UV-vis spectra of the κ-CG film, the cyt *c* monolayered on κ-CG film and 8-bilayer κ-CG/cyt c on κ-CG film. UV-vis spectra of the cyt *c* solution (20 μM) were also taken for comparison (Fig. 9 inset). As shown from the figure, the cyt c solution exhibited a clear absorption peak around 408 nm. The κ-CG film did not show any absorption peak in the examined spectral region. However, the cyt *c* monolayered κ-CG film and the 8- bilayer κ-CG/cyt *c* film showed an absorption peak around 408 nm. These results indicate that the cyt *c* is assembled on κ-CG film. When the absorption peak intensities of the two films (the cyt *c* monolayered κ-CG film and the 8-bilayer κ-CG/cyt *c* carrying the κ-CG film) are compared, it is seen that the peak intensity of the 8-bilayer κ-CG/cyt *c* film is higher. This difference shows that the cyt *c* and κ-CG can be deposited via the LBL assembly technique.

Fig.9

4. Conclusion

In this study, some parameters related to the electrostatic interaction between κ-CG and cyt *c* were optimized to build up a multilayer κ-CG/cyt *c* electroactive artificial film on a gold electrode. The peak currents of the multilayer film on the electrode showed an increase with the addition of each layer of cyt *c*. The κ-CG/cyt *c* multilayer film exhibited direct electron exchange between cyt *c* layers in a surface-fixed state. With an 8-bilayer κ-CG/cyt *c* film, the content of the immobilized cyt *c* was found to be 15 times higher than in a monolayer system. In addition, multilayer protein film formation was confirmed by electrochemical impedance spectroscopy, ellipsometry, and UV-vis absorption spectroscopy. This multilayer film can be used as an immobilization platform for some redox enzymes in the preparation of the third-generation biosensors in which direct electron transfer is accomplished using no diffusional electron transport mediator [60].

Acknowledgment

This work was supported by the Research Foundation of Kırıkkale University (2012-25).

References

[1] X-W. Shi, L. Qiu, Z. Nie, L. Xiao, G. F. Payne, Y. Du, Protein addressing on patterned microchip by coupling chitosan electrodeposition and 'electro-click' chemistry, Biofabrication 5 (2013) 041001.
[2] C. Schulz, R. Ludwig, L. Gorton, Polyethyleneimine as a promoter layer for the immobilization of cellobiose dehydrogenase from myriococcum thermophilum on graphite electrodes, Anal. Chem., 86 (2014) 4256-4263.
[3] S. T. Koev, P. H. Dykstra, X. Luo, G. W. Rubloff, W. E. Bentley, G. F. Payne, R Ghodssi, Chitosan: an integrative biomaterial for lab-on-a-chip devices, Lab on a Chip, 10 (2010) 3026-3042.
[4] E. Kim, Y. Xiong, Y. Cheng, H. C. Wu, Y. Liu, B. H. Morrow, H. Ben-Yoav, R. Ghodssi, G. W. Rubloff, J. Shen, W. E. Bentley, X. Shi, G. F. Payne, Chitosan to connect biology to electronics: fabricating the bio-device interface and communicating across this interface, Polymers, 7 (2015) 1-46.
[5] F. R. R. Teles, L. P. Fonseca, Applications of polymers for biomolecule immobilization in electrochemical biosensors, Mater. Sci. Eng. C, 28 (2008) 1530-1543.
[6] M. Zhang, C. Mullens, W. Gorski, Coimmobilization of dehydrogenases and their cofactors in electrochemical biosensors, Anal. Chem., 79 (2007) 2446-2450.
[7] F. Lisdat, R. Dronov, H. Möhwald, F. W. Scheller, D. G. Kurth, Self-assembly of electro-active protein architectures on electrodes for the construction of biomimetic signal chains, Chem. Commun., 0 (2009) 274-283.
[8] P. O. Saboe, E. Conte, M. Farell, G. C. Bazan, M. Kumar, Biomimetic and bioinspired approaches for wiring enzymes to electrode interfaces, Energy Environ. Sci., 10 (2017) 14-42.
[9] A. R. Puente-Santiago, D. Rodríguez-Padron, X. Quan, M. J. M. Batista, L. O. Martins, S. Verma, R. S. Varma, J. Zhou, R. Luque, Unprecedented wiring efficiency of sulfonated graphitic carbon nitride materials: toward high-performance amperometric recombinant Cot A laccase biosensors, ACS Sustainable Chem. Eng., 7 (2019) 1474-1484.

[10] Y. S. Lee, S. Baek, H. Lee, S. S. Reginald, Y. Kim, H. Kang, I. Choi, I. S. Chang, Construction of uniform monolayer and orientation tunable enzyme electrode by a synthetic glucose dehydrogenase without electron-transfer subunit via optimized site-specific gold-binding peptide capable of direct electron transfer, ACS Appl. Mater. Interfaces, 10 (2018) 28615−28626.
[11] P. Bollella, Y. Hibino, K. Kano, L. Gorton, R. Antiochia, Enhanced direct electron transfer of fructose dehydrogenase rationally immobilized on a 2-aminoanthracene diazonium cation grafted single-walled carbon nanotube based electrode, ACS Catal., 8 (2018) 10279−10289.
[12] Y. Liu, J. Zhang, Y. Cheng, S. P. Jiang, Effect of carbon nanotubes on direct electron transfer and electrocatalytic activity of ımmobilized glucose oxidase, ACS Omega, 3 (2018) 667−676.
[13] J. M. Goran, J. L. Lyon, K. J. Stevenson, Amperometric detection of L-lactate using nitrogen-doped carbon nanotubes modified with lactate oxidase, Anal. Chem., 83 (2011) 8123-8129.
[14] Th. Balkenhohl, S. Adelt, R. Dronov, F. Lisdat, Oxygen-reducing electrodes based on layer-by-layer assemblies of cytochrome c and laccase, Electrochem. Commun., 10 (2008) 914-917.
[15] Z. S. Aghamiri, M. Mohsennia, H-A. Rafiee-Pour, Immobilization of cytochrome *c* and its application as electrochemical biosensors, Talanta, 176 (2018) 195-207.
[16] P. Manickam, A. Kaushik, C. Karunakaran, S. Bhansali, Recent advances in cytochrome *c* biosensing technologies, Biosens. Bioelectron., 87 (2017) 654-668.
[17] M. C. Leopold, E. F. Bowden, Influence of gold substrate topography on the voltammetry of cytochrome *c* adsorbed on carboxylic acid terminated self-assembled monolayers, Langmuir, 18 (2002) 2239-2245.
[18] S-F. Wang, T. Chen, Z-L. Zhang, X-C. Shen, Z-X. Lu, D-W. Pang, K-Y. Wong, Direct electrochemistry and electrocatalysis of heme proteins entrapped in agarose hydrogel films in room-temperature ionic liquids, Langmuir, 21 (2005) 9260-9266.
[19] C. Xiang, Y. Zou, L-X. Sun, F. Xu, Direct electrochemistry and electrocatalysis of cytochrome c immobilized on gold nanoparticles–chitosan–carbon nanotubes-modified electrode, Talanta, 74 (2007) 206-211.
[20] L. M. Moretto, P. Bertoncello, F. Vezzà, P. Ugo, Electrochemistry of cytochrome c incorporated in Langmuir–Blodgett films of Nafion® and Eastman AQ 55®, Bioelectrochemistry, 66 (2005) 29-34.
[21] S. H. Takahashi, S. I. C. De Torresi, Nitric oxide sensing by cytochrome c bonded to a conducting polymer modified glassy carbon electrode, Synth. Met., 159 (2009) 2159-2161.
[22] W. Xu, Z. Wang, L. Shi, Y. Ma, S. Yuan, L. Sun, Y. Zhao, M. Zhang, J. Zhu, Layer-by-layer deposition of organic–inorganic hybrid multilayer on microporous polyethylene separator to enhance the electrochemical performance of lithium-ion battery, ACS Appl. Mater. Interfaces, 7 (2015) 20678-20686.
[23] F. N. Crespilho, V. Zucolotto, O. N. Oliveira Jr., F. C. Nart, Electrochemistry of layer-by-layer films: a review, Int. J. Electrochem. Sci., 1 (2006) 194-214.
[24] J. J. Richardson, J. Cui, M. Björnmalm, J. A. Braunger, H. Ejima, F. Caruso, Innovation in layer-by-layer assembly, Chem. Rev., 116 (2016) 14828-14867.

[25] M. K. Beissenhirtz, F. W. Scheller, F. Lisdat, A superoxide sensor based on a multilayer cytochrome *c* electrode, Anal. Chem., 76 (2004) 4665-4671.
[26] N. Mirkin, J. Jaconcic, V. Stojanoff, A. Moreno, High resolution X-ray crystallographic structure of bovine heart cytochrome *c* and its application to the design of an electron transfer biosensor, Proteins, 70 (2008) 83-92.
[27] T-Y. Lee, H-J. Kim, J-O. Moon, Y-B. Shim, Determination of cytochrome *c* with cellulose – DNA modified carbon paste electrodes, Electroanalysis, 16, (2004) 821-826.
[28] D. Sarauli, J. Tanne, C. Xu, B. Schulz, L. Trnkova, F Lisdat, Insights into the formation and operation of polyaniline sulfonate/cytochrome *c* multilayer electrodes: contributions of polyelectrolytes' properties, Phys. Chem. Chem. Phys., 12 (2010) 14271-14277.
[29] D. Sarauli, J. Tanne, D. Schäfer, I. W. Schubart, F. Lisdat, Multilayer electrodes: Fully electroactive cyt *c* on gold as a part of a DNA/protein architecture, Electrochem. Commun., 11 (2009) 2288-2291.
[30] R. Spricigo, R. Dronov, F. Lisdat, S. Leimkühler, F. W. Scheller, U. Wollenberger, Electrocatalytic sulfite biosensor with human sulfite oxidase co-immobilized with cytochrome *c* in a polyelectrolyte-containing multilayer, Anal. Bioanal. Chem., 393 (2009) 225-233.
[31] S. C. Feifel, A. Kapp, R. Ludwig, L. Gorton, F. Lisdat, Electrocatalytically active multi-protein assemblies using nanoscaled building blocks, RSC Adv., 3 (2013) 3428-3437.
[32] F. Wegerich, P. Turano, M. Allegrozzi, H. Möhwald, F Lisdat, Electroactive multilayer assemblies of bilirubin oxidase and human cytochrome c mutants: insight in formation and kinetic behavior, Langmuir, 27 (2011) 4202-4211.
[33] S. C. Feifel, A. Kapp, F. Lisdat, Electroactive nanobiomolecular architectures of laccase and cytochrome c on electrodes: Applying silica nanoparticles as artificial matrix, Langmuir, 30 (2014) 5363-5367.
[34] L. Gorton, A. Lindgren, T. Larsson, F.D. Munteanu, T. Ruzgas, I. Gazaryan, Direct electron transfer between heme-containing enzymes and electrodes as basis for third generation biosensors, Anal. Chim. Acta, 400 (1999) 91-108.
[35] S. C. Feifel, R. Ludwig, L. Gorton, F. Lisdat, Catalytically active silica nanoparticle-based supramolecular architectures of two proteins – cellobiose dehydrogenase and cytochrome c on electrodes, Langmuir, 28 (2012) 9189-9194.
[36] L. Li, R. Ni, Y. Shao, S. Mao, Carrageenan and its applications in drug delivery, Carbohydr. Polym., 103 (2014) 1-11.
[37] K. O. Ribeiro, M. I. Rodrigues, E. Sabadini, R. L. Cunha, Mechanical properties of acid sodium caseinate-κ-carrageenan gels: effect of co-solute addition, Food Hydrocoll., 18 **(**2004) 71-79
[38] C. Alvarez-Lorenzo, B. Blanco-Fernandez, A. M. Puga, A. Concheiro, "Crosslinked ionic polysaccharides for stimuli-sensitive drug delivery, Adv. Drug Deliv. Rev., 65 (2013) 1148-1171.
[39] S. Rudhziah, A. Ahmad, I. Ahmad, N. S. Mohamed, Biopolymer electrolytes based on blend of kappa-carrageenan and cellulose derivatives for potential application in dye sensitized solar cell, Electrochim. Acta, 175 (2015) 162-168.
[40] H. C. Yu, H. Zhang, K. Ren, Z. Ying, F. Zhu, J. Qian, J. Ji, Z. L. Wu, Q. Zheng, Ultrathin κ-carrageenan/chitosan hydrogel films with high toughness and antiadhesion property, ACS Appl. Mater. Interfaces, 10 (2018) 9002-9009.

[41] B. Ge, F. Lisdat, Superoxide sensor based on cytochrome c immobilized on mixed-thiol SAM with a new calibration method, Anal. Chim. Acta, 454 (2002) 53-64.
[42] E. Katz, D. D. Schlereth, H-L. Schmidt, Electrochemical study of pyrroloquinoline quinone covalently immobilized as a monolayer onto a cystamine-modified gold electrode, J. Electroanal. Chem., 367 (1994) 59-70.
[43] M. K. Beissenhirtz, F. W. Scheller, W. F. M. Stöcklein, D. G. Kurth, H. Möhwald, F. Lisdat, Electroactive cytochrome *c* multilayers within a polyelectrolyte assembly, Angew. Chem. Int. Ed., 43 (2004) 4357-4360.
[44] C. Wettstein, H. Möhwald, F. Lisdat, Coupling of pyrroloquinoline quinone dependent glucose dehydrogenase to (cytochrome c/DNA)-multilayer systems on electrodes, Bioelectrochemistry, 88 (2012) 97-102.
[45] C. Wettstein, K. Kano, D. Schafer, U. Wollenberger, F. Lisdat, Interaction of flavin-dependent fructose dehydrogenase with cytochrome *c* as basis for the construction of biomacromolecular architectures on electrodes, Anal. Chem., 88 (2016) 6382-6389.
[46] F. Lisdat, Trends in the layer-by-layer assembly of redox proteins and enzymes in bioelectrochemistry, Curr. Opin. Electrochem., 5, (2017) 165-172.
[47] M. J. Eddowes, H. A. O. Hill, Electrochemistry of horse heart cytochrome *c*, J. Am. Chem. Soc., 101 (1979) 4461-4464.
[48] F. Wegerich, P. Turano, M. Allegrozzi, H. Möhwald, F. Lisdat, Cytochrome *c* mutants for superoxide biosensors, Anal. Chem., 81 (2009) 2976-2984.
[49] N. M. Alves, C. Picart, J. F. Mano, Self assembling and crosslinking of polyelectrolyte multilayer films of chitosan and alginate studied by QCM and IR spectroscopy, Macromol. Biosci., 9 (2009) 776-785.
[50] W. Yuan, H. Dong, C. M. Li, X. Cui, L. Yu, Z. Lu, Q. Zhou, pH-Controlled construction of chitosan/alginate multilayer film: characterization and application for antibody immobilization, Langmuir, 23 (2007) 13046-13052.
[51] J. Wallerstein, U. Weininger, M. A. I. Khan, S. Linse, M. Akke, Site-specific protonation kinetics of acidic side chains in proteins determined by pH-dependent carboxyl ^{13}C NMR relaxation, J. Am. Chem. Soc., 137 (2015) 3093-3101.
[52] M. Yiğitoğlu, Z. Temoçin, Removal of benzidine-based azo dye from aqueous solution using amide and amine-functionalized poly(ethylene terephthalate) fibers, Fiber. Polym., 11 (2010) 996-1002.
[53] E. Laviron, General expression of the linear potential sweep voltammogram in the case of diffusionless electrochemical systems, J. Electroanal. Chem., 101 (1979) 19–28.
[54] M. Eguílaz, A. Gutiérrez, G. Rivas, Non-covalent functionalization of multi-walled carbon nanotubes with cytochrome c: Enhanced direct electron transfer and analytical applications, Sens. Actuators B, 225 (2016) 74–80.
[55] Z. S. Aghamiri, M. Mohsennia, H. A. Rafiee-Pour, Fabrication and characterization of cytochrome c-immobilized polyaniline/multi-walled carbon nanotube composite thin film layers for biosensor applications, Thin Solid Films, 660 (2018) 484–492.
[56] M. Shamsipura, A. Pashabadia, F. Molaabasib, S. Hosseinkhani, Impedimetric monitoring of apoptosis using cytochrome-aptamer bioconjugated silver nanocluster, Biosens. Bioelectron., 90 (2017) 195–202.

[57] Y. Song, L. Wan, Y. Wang, S. Zhao, H. Hou, L. Wang, Electron transfer and electrocatalytics of cytochrome c and horseradish peroxidase on DNA modified electrode, Bioelectrochemistry 85 (2012) 29-35.
[58] M. V. Bracamonte, O. E. L. Pérez, M. L. Teijelo, G. A. Rivas, N. F. Ferreyra, Quaternized chitosan mediated assembly of gold nanoparticles multilayers, Electrochim. Acta, 146 (2014) 178–185.
[59] J. N. Hilfiker, G. K. Pribil, R. Synowicki, A. C. Martin, J. S. Hale, Spectroscopic ellipsometry characterization of multilayer optical coatings, Surf. Coat. Technol., 357 (2019) 114–121.
[60] S. C. Feifel, K. R. Stieger, A. Kapp, D. Weber, M. Allegrozzi, M. Piccioli, P. Turano, F. Lisdat, Insights into interprotein electron transfer of human *cytochrome c* variants arranged in multilayer architectures by means of an artificial silica nanoparticle matrix, ACS Omega, 1 (2016) 1058-1066.

Figure captions

Schematic 1. The successive incubation steps for construction of the multilayer κ-CG/cyt *c* film on cyt *c* monolayered gold surface.

Fig. 1. Cyclic voltammogram of the immobilized cyt *c* monolayer on the gold electrode (a). Stability of the oxidation and reduction peak currents of the cyt *c* monolayer over multiple cycles (b).

Fig. 2. Effect of solution pH values on self-assembly of κ-CG and cyt *c* (constructed structure: cyt *c*/[κ-CG/cyt *c*]$_2$, ▬ pH 4.0, ▬ pH 5.0, ▬ pH 6.0, ▬ pH 7.0, ▬ cyt *c* monolayer), voltammograms of the multilayer electroactive cyt *c* (a). Amounts of electroactive cyt *c* on the electrode surface (b). Effect of incubation method on the immobilization of electroactive cyt *c* (▬ incubated in the mixture of cyt *c* and κ-CG, ▬ cyt *c* monolayer, ▬ LBL [κ-CG/cyt *c*]$_2$) (c).

Fig. 3. Effect of incubation time on self-assembly of κ-CG and cyt *c* (constructed structure: cyt *c*/[κ-CG/cyt *c*]$_2$), voltammograms of the multilayer electroactive cyt *c* (▬ 2.5 min, ▬ 5 min, ▬ 10 min, ▬ 20 min) (a). Amounts of electroactive cyt *c* on the electrode surface (b).

Fig. 4. Effect of κ-CG concentration on the construction of multilayer assembly (constructed structure: cyt *c*/[κ-CG/cyt *c*]$_3$) voltammograms of the multilayer electroactive cyt *c* (▬ 0.1 mg mL^{-1}, ▬ 0.25 mg mL^{-1}, ▬ 0.5 mg mL^{-1}, ▬ 1 mg mL^{-1}) (a). Amounts of electroactive cyt *c* on electrode surface (b).

Fig. 5. κ-CG/cyt *c* multilayer system (constructed structure: cyt *c*/[κ-CG/cyt *c*]$_{2\text{-}8}$) voltammograms of the immobilized electroactive cyt *c* in multilayer system (▬ cyt *c* monolayer, ▬ cyt *c*/[κ-CG/cyt *c*]$_2$, ▬ cyt *c*/[κ-CG/cyt *c*]$_4$, ▬ cyt *c*/[κ-CG/cyt *c*]$_6$, ▬ cyt *c*/[κ-CG/cyt *c*]$_8$), inset: stability of the oxidation and reduction peaks currents of the 8-bilayer κ-CG/cyt *c* film over multiple cycles (a). Amounts of the electroactive cyt *c* on the electrode surface (b). Peak separations for 2–8 κ-CG/cyt *c* bilayers (c).

Fig. 6. The variation of the anodic and cathodic peaks potentials with respect to the scan rate in the cyclic voltammograms. (constructed structure: cyt *c*/[κ-CG/cyt *c*]$_4$, scan rate: ▬ 0.05, ▬ 0.1, ▬ 0.2, ▬ 0.4, ▬ 0.5, ▬ 0.8, ▬ 1.0 V s^{-1}) inset: the variation of the anodic and cathodic peaks currents.

Fig. 7. Nyquist plots of the bare gold electrode (••••), monolayered cyt *c* (◆◆◆), 2-bilayer κ-CG/cyt *c* (▬ ▬ ▬), 4-bilayer κ-CG/cyt *c* (▲▲▲), 6-bilayer κ-CG/cyt *c* (■■■) and 8-bilayer κ-CG/cyt *c* (●●●), inset: the Randles circuit.

Fig. 8. Ellipsometric measurements, change of Ψ with wavelength (bare gold ▬ · ·, 4-bilayer κ-CG/cyt *c* film ▬ ▬ ▬**,** and 8-bilayer κ-CG/cyt *c* film ▬▬).

Fig. 9. UV-vis spectra (κ-CG film ▬▬, cyt *c* monolayered κ-CG film ▬▬, 8-bilayer κ -CG/cyt *c* carrying κ-CG film ▬▬, inset: the UV-vis spectra of 20 μM cyt *c* solution.

Highlights

- κ-CG was employed for multilayer immobilization of the electroactive cyt *c*.
- The electron transport between cyt *c* layers was established.
- The cyt *c* content was increased by 15 times with multilayer film formation.